International Journal of Multidisciplinary Research and Growth Evaluation.

GIS Based Landslide Susceptibility Modelling in Anambra State Nigeria Using MEREC Objective Weighting

Igbokwe OI [1*], Ono MN [2], Emengini EJ [3], Okafor OC [4], Udoudo NP [5]
[1-5] Department of Surveying and Geoinformatics, Nnamdi Azikiwe University Awka, Anambra State, Nigeria

* Corresponding Author: **Igbokwe OI**

Article Info

ISSN (Online): 2582-7138
Volume: 07
Issue: 06
Received: 20-08-2026
Accepted: 22-09-2026
Published: 24-10-2026
Page No: 237-248

Abstract
Landslide susceptibility was modelled across Anambra State, Nigeria, using the Method based on the Removal Effects of Criteria (MEREC) and seven spatial criteria: slope, rainfall, topographic wetness index (TWI), drainage density, normalized difference vegetation index (NDVI), local relief derived from elevation, and aspect. The seven conditioning-factor rasters and state boundary were harmonized to a 30 m WGS 84 / UTM Zone 32N grid. MEREC weights were calculated from all 5,088,684 valid cells covering 4,579.8156 km². Rainfall received the highest weight (0.190530), followed by drainage density (0.183486), NDVI (0.176849), TWI (0.164416), local relief (0.150237), and slope (0.134483); aspect had a zero weight because its classes were assigned a neutral score. The continuous index ranged from 0.059135 to 0.776930 and was classified into five quantile-based susceptibility zones. High and Very High zones together covered 1,831.9266 km². Orumba North recorded the largest Very High area (133.4772 km²), while Nnewi South had the highest within-LGA Very High proportion (48.92%). Sensitivity analysis showed that omission of rainfall or local relief changed zone assignments, demonstrating the influence of these criteria on the final spatial pattern. The analysis provides a spatially explicit, reproducible MEREC-based susceptibility surface and LGA summaries for environmental screening.

Keywords: Anambra State, landslide susceptibility, MEREC, GIS, topographic wetness index, local relief, spatial analysis

1. Introduction

Landslide susceptibility mapping identifies the relative spatial propensity for slope failure from the distribution of terrain, geological, hydrological, climatic, vegetation, and human-related conditions. It provides a basis for comparing locations and prioritizing detailed investigation. Susceptibility differs conceptually from hazard, which incorporates the probability of occurrence within a defined time period, and from risk, which combines hazard with exposure and potential consequences. Statistical, multicriteria, and machine-learning approaches are widely used to represent landslide conditioning factors and map their spatial combinations (Reichenbach *et al*., 2018; Zhao *et al*., 2023) [15, 25]. Recent reviews document continued development in remote sensing and geospatial modelling, including conventional and advanced techniques for landslide detection and susceptibility assessment (Akosah *et al*., 2024; Li *et al*., 2024; Kudaibergenov *et al*., 2025; Shafapourtehrany *et al*., 2026) [2, 11, 12, 19].

Anambra State presents a relevant setting for this type of spatial assessment. The Nanka area has a documented history of damaging slope failures associated with rainfall infiltration, steep slopes, and contrasts between poorly consolidated sands and less permeable silty clay units (Igwe & Una, 2019) [9]. Research on groundwater conditions in southeastern Nigeria has also shown how changing groundwater levels can influence shallow slope stability (Ibeh, 2020) [8]. More recently, geospatial modelling in southern Anambra has mapped landslide-prone areas using terrain, rainfall, vegetation, drainage, and geological variables (Nwazelibe & Egbueri, 2024) [14]. Together, these studies establish the regional relevance of combining terrain, hydrological, rainfall, and vegetation information in a state-wide susceptibility framework.

The conditioning factors selected for a susceptibility model represent distinct processes and spatial scales. Slope and local relief describe terrain form; rainfall and TWI characterize water input and potential moisture convergence; drainage density describes the organization of the drainage network; and NDVI represents vegetation condition. Elevation and vegetation responses can vary across landscapes, while terrain wetness estimates depend on flow-routing algorithms and grid resolution (Riihimäki *et al*., 2021; Winzeler *et al*., 2022) [16, 22]. Remote sensing products support broad-area analysis, but their interpretation depends on sensor characteristics, surface-reflectance processing, and temporal consistency (Roy *et al*., 2016; Vermote *et al*., 2016; Claverie *et al*., 2018; Wulder *et al*., 2019) [4, 18, 21, 23]. CHIRPS provides a long-term precipitation record that supports regional rainfall analysis (Funk *et al*., 2015) [6].

Objective weighting offers a transparent way to derive criterion importance from the spatial decision matrix. MEREC calculates a criterion's weight from the effect its removal has on the overall performance of alternatives (Keshavarz-Ghorabaee *et al*., 2021) [10]. In a raster application, valid cells form the alternatives and conditioning factors form the criteria. The method is distinct from assigning weights through expert pairwise comparisons, and comparative multicriteria research shows that weighting choices influence spatial prioritization outcomes (Mahmoodi *et al*., 2023) [13]. MEREC is therefore applied in this study as the sole criterion-weighting method.

This study develops and interprets a MEREC-based landslide susceptibility model for Anambra State using an aligned raster workflow and all valid analysis cells. It examines the spatial distributions of the factors, derives objective MEREC weights, calculates a continuous landslide susceptibility index, classifies the index into five zones, and summarizes zone areas for the 21 Local Government Areas. The analysis follows established geospatial practice for raster preparation and landslide conditioning-factor assessment (Alvioli *et al*., 2016; Gorelick *et al*., 2017) [3, 7]. Its LGA summaries and factor maps extend local landslide research by presenting a consistent state-wide spatial assessment. Research on susceptibility modelling increasingly emphasizes spatially aware model evaluation and transparent performance reporting (Roberts *et al*., 2017; Valavi *et al*., 2019; Abdelkader & Csámer, 2025) [1, 17, 20].

2. Materials and Methods

2.1. Study Area

Anambra State is located in southeastern Nigeria on the eastern plains of the River Niger. Its landscape comprises low-lying plains and rolling, dissected uplands, with hills, lakes, forests, and caves forming part of its varied physical setting (Anambra State Government, n.d.; Igwe & Una, 2019) [9]. The study area covers 4,592.5422 km² based on the state polygon used in this analysis and includes 21 Local Government Areas. The contrast between lower-relief areas and dissected terrain provides the regional setting for the landslide susceptibility assessment.

All spatial data were processed in WGS 84 / UTM Zone 32N (EPSG:32632), which provides metre-based coordinates for raster alignment and area calculation. Raster-cell area and vector-boundary area were calculated separately to maintain consistent area accounting.

2.2. Input Data and Factor Preparation

The analysis used seven factor rasters and the Anambra State administrative boundary. Table 1 summarizes the input factors, raster dimensions, native value ranges, NoData values, and stated data sources. The raster layers had a nominal 30 m cell spacing and were delivered with differing dimensions and grid origins. Input metadata and accompanying files were reviewed before harmonization; the original datasets were retained unchanged.

Table 1: Input factor inventory and raster properties.

Factor	Rows × columns	Native range	NoData
Aspect	4006 × 2789	-1.000 to 359.519	Float minimum
Drainage Density	3990 × 2779	0.015 to 1.978	Float minimum
Elevation	4006 × 2789	5.000 to 388.000	32767
NDVI	3990 × 2779	-0.259 to 0.652	Float minimum
Rainfall	4142 × 2968	2,344.000 to 3,357.000	32767
Slope	4006 × 2789	0.000 to 43.120	Float minimum
TWI	3990 × 2780	5.795 to 30.341	Float minimum

NDVI was used as a vegetation-condition factor. It is conventionally calculated as (NIR − Red)/(NIR + Red); for Landsat 8 OLI, the near-infrared and red bands are bands 5 and 4, respectively. Lower NDVI values were oriented toward greater susceptibility to represent reduced vegetation cover. Landsat surface reflectance products and harmonized satellite imagery support consistent vegetation-index analysis when radiometric and cloud-screening procedures are applied (Roy *et al*., 2016; Vermote *et al*., 2016; Claverie *et al*., 2018) [4, 18, 21].

The CHIRPS 2025 rainfall raster represented the spatial rainfall pattern. Pixel values ranged from 2,344 to 3,357 and were retained as a continuous relative rainfall surface for raster overlay. CHIRPS is a satellite and station-based precipitation dataset developed for spatial and temporal climate analysis (Funk *et al*., 2015) [6].

Elevation and slope were obtained from the stated SRTM source, while drainage density was treated as a continuous measure of drainage-network concentration. SRTM elevation is expressed in metres and slope in degrees. The TWI layer was recalculated from the DEM because the topographic wetness index is derived from terrain slope and upslope contributing area. Factor value ranges on the final analysis mask are presented in Table 2.

2.3. Raster Harmonization and Analysis Mask

Elevation defined the reference grid, comprising 4,006 rows and 2,789 columns, 30 m cells, and an extent of 235,510.925–319,180.925 m E and 629,483.466–749,663.466 m N. All layers were processed in EPSG:32632. Continuous rasters were aligned using bilinear resampling; aspect was aligned using nearest-neighbour resampling to preserve its circular direction values.

The Anambra State polygon was rasterized using cell-centre inclusion. Non-finite and NoData cells were excluded, together with values outside the valid ranges for slope, NDVI, rainfall, drainage density, and aspect. The final common mask contained 5,088,684 cells. Harmonized factor rasters shared a common extent, cell size, origin, projection, and valid-data mask.

2.4. DEM Derived Topographic Wetness Index

The TWI was derived from the SRTM elevation model using flow accumulation and local slope. This index represents the potential for topographic moisture convergence and is commonly expressed as the natural logarithm of specific contributing area divided by the tangent of slope. Its values depend on the flow-routing method and raster resolution (Riihimäki *et al*., 2021; Winzeler *et al*., 2022) [16, 22].

A single-flow D8 routing procedure was applied to the DEM. Cells were routed to the steepest downslope neighbour, with diagonal distance accounted for; flat cells followed the priority-flood discovery tree. Flow accumulation was calculated in reverse traversal order. The same 30 m DEM was used to calculate local slope for the TWI equation.

$$a_i = A_i/b = (C_i \times 900m^2)/30m = 30C_im \quad (1)$$

$$TWI_i = ln[a_i/max(tan\beta_i, 0.001)] \quad (2)$$

Here, C_i is the accumulated contributing-cell count, a_i is specific contributing area using a 30 m contour-width convention, and β_i is local slope in radians. The 0.001 minimum tangent value stabilizes calculations on near-flat terrain. The resulting TWI raster was aligned with the other factors and entered into the MEREC decision matrix.

2.5. Factor Response and Standardization

Factor responses were oriented so that higher standardized values represented greater landslide susceptibility. Slope, rainfall, TWI, and drainage density were treated as increasing-response factors. NDVI was reversed so that lower vegetation greenness corresponded to higher susceptibility scores. Table 2 summarizes the raw ranges and response directions applied to the model.

Absolute elevation was transformed to local relief to represent local terrain dissection. Local relief was calculated as the difference between maximum and minimum elevation within a 33 × 33-cell moving window, corresponding to a 990 m neighbourhood. Higher local relief was treated as a greater susceptibility contribution. This transformation retains terrain position and contrast while avoiding an assumed monotonic response to absolute altitude.

Aspect was classified into eight 45° compass sectors and a flat-surface class. Each class received a neutral standardized value of 0.5005 because the available spatial information did not support a defensible statewide ordering of compass directions. The constant aspect column consequently produced a zero MEREC removal effect and zero final weight.

Table 2: Factor ranges and susceptibility response directions on the analysis mask.

Criterion	Original range	Response and direction
Slope	0.000 to 43.120	increasing
Rainfall	2,344.000 to 3,357.000	Increasing rainfall pattern
TWI	3.492 to 24.331	increasing moisture potential
Drainage Density	0.023 to 1.977	increasing erosion proxy
NDVI	-0.254 to 0.635	decreasing vegetation proxy
Elevation / local relief	5.000 to 388.000	increasing 990 m local relief; altitude nonmonotonic
Aspect	-1.000 to 359.519	eight compass classes and flat; all neutral

$$u_{ij} = clip[(v_{ij} - P1_j)/(P99_j - P1_j), 0,1] \quad (3)$$

$$u_i, NDVI = 1 - u_i, NDVI; \quad x_{ij} = 0.001 + 0.999u_{ij} \quad (4)$$

In Equation 3, v_{ij} is the observed factor response, including local relief for the elevation-derived criterion, and $P1_j$ and $P99_j$ are the first and ninety-ninth percentiles. Values were clipped to the interval 0–1, and NDVI was reversed once before transformation. Equation 4 scaled each varying factor to positive values between 0.001 and 1.000 for the logarithmic MEREC calculations. Aspect was held constant at 0.5005.

2.6. MEREC Criterion Weighting and Susceptibility Index

The decision matrix X contained 5,088,684 valid raster cells and seven factor columns: slope, rainfall, TWI, drainage density, NDVI, local relief, and aspect. All valid cells were included in the MEREC calculations. The criterion weights were derived from the removal effects of each factor on overall cell performance, following the original MEREC method (Keshavarz-Ghorabaee *et al*., 2021) [10].

Following direction standardization, all factors were treated as benefit criteria, for which higher x_{ij} values represent a greater susceptibility contribution. The MEREC normalization, removal-performance calculation, effect summation, and weight normalization are expressed in Equations 5–8.

$$n_{ij} = min_i(x_{ij})/x_{ij} \quad (5)$$

for each direction-standardized criterion

$$S_i = ln\left[1 + (1/m)\Sigma_j\left|ln(n_{ij})\right|\right], m = 7 \quad (6)$$

$$S_i(-j) = ln[1 + (1/m)\Sigma_k \neq {}_j|ln(n_{ik})|] \quad (7)$$

$$E_j = \Sigma_i|S_i(-j) - S_i|; w_j = E_j/\Sigma_k E_k \quad (8)$$

$$LSI_i = \Sigma_j w_j x_{ij} \quad (9)$$

In these equations, n_{ij} is the normalized value, S_i is the overall performance of cell I, $S_i(-j)$ is its performance with criterion

j removed, E_j is the removal effect, and w_j is the normalized MEREC weight. The denominator m remains seven in the removal calculation, following the original formulation. The final landslide susceptibility index (LSI) is the weighted sum of the positive, susceptibility-oriented factor values.

2.7. Susceptibility Classification and LGA Summaries

The continuous LSI was classified into Very Low, Low, Moderate, High, and Very High zones using the 20th, 40th, 60th, and 80th percentiles of the saved index raster. Class intervals and area statistics are presented in Table 4. The quantile method provides five relative spatial classes across the modelled area.

Table 4: Continuous-index thresholds and areas of the five susceptibility zones.

Zone	Index interval	Area km²
Very Low	[0.059135, 0.301204]	915.9633
Low	(0.301204, 0.348044]	915.9633
Moderate	(0.348044, 0.389910]	915.9624
High	(0.389910, 0.439736]	915.9633
Very High	(0.439736, 0.776930]	915.9633

Zone areas were calculated from the number of classified cells multiplied by the 900 m² cell area. Raster cells were assigned to LGAs using their centre coordinates. Table 5 reports zone area by LGA and the proportion of each LGA classified as Very High. Classified zones were also polygonized and checked against raster cell totals.

Table 5: Susceptibility-zone area by Local Government Area in square kilometres.

LGA	Very Low	Low	Moderate	High	Very High	VH %
Aguata	8.04	18.17	29.85	48.21	57.54	35.56
Anambra East	25.56	81.27	96.92	92.05	82.84	21.88
Anambra West	395.19	193.89	93.88	44.82	9.68	1.31
Anaocha	4.32	14.53	22.98	29.18	33.92	32.33
Awka North	81.35	124.61	107.50	59.29	14.26	3.69
Awka South	3.57	21.42	48.18	59.55	38.02	22.27
Ayamelum	263.80	166.79	90.72	36.75	8.11	1.43
Dunukofia	1.66	12.97	21.28	16.68	5.80	9.93
Ekwusigo	5.07	16.69	26.44	33.15	25.61	23.95
Idemili North	5.38	14.76	18.54	23.29	25.35	29.03
Idemili South	7.32	14.50	21.01	30.61	37.29	33.67
Ihiala	9.15	29.04	41.69	55.31	85.28	38.68
Njikoka	3.90	16.32	22.51	24.59	26.42	28.19
Nnewi North	0.98	4.95	10.29	21.38	26.95	41.75
Nnewi South	1.88	9.60	24.95	49.27	82.08	48.92
Ogbaru	73.09	99.50	86.82	63.39	72.57	18.35
Onitsha North	3.17	4.20	4.17	8.17	8.23	29.45
Onitsha South	6.08	5.83	2.58	1.36	1.09	6.43
Orumba North	13.35	36.67	71.29	107.42	133.48	36.85
Orumba South	2.20	20.15	43.58	64.45	99.06	43.18
Oyi	0.89	10.09	30.77	47.02	42.38	32.31

2.8. Sensitivity Analysis

Four sensitivity scenarios were evaluated: omission of rainfall, omission of local relief, omission of both factors, and use of a 0.01 rather than 0.001 positive floor. MEREC weights and quantile class boundaries were recalculated for each scenario. Spearman correlation with the baseline index, class agreement, and retention of baseline Very High cells were used to summarize sensitivity. These results are reported in Table 6.

Table 6: Sensitivity of recalculated scenarios relative to the baseline.

Scenario	Spearman ρ	Same class %	Baseline VH retained %
No rainfall	0.8456	50.96	76.14
No local relief	0.8896	53.87	68.29
No rainfall or relief	0.5799	31.01	49.31
Positive floor 0.01 instead of 0.001	0.9991	95.66	97.00

The analysis was implemented with Python and the Rasterio/GDAL, NumPy, SciPy, GeoPandas, and Matplotlib libraries. Processing scripts, parameter settings, raster outputs, and area summaries were retained for reproducibility. Cloud-based geospatial platforms and slope-unit segmentation are established options for large-area and geomorphologically based analyses (Gorelick *et al.*, 2017; Alvioli *et al.*, 2016) [3, 7], while the present study used a common pixel grid.

3. Results

3.1. Factor Distributions and Analysis Coverage

The common analysis mask covered 4,579.8156 km², equivalent to 99.7229% of the vector boundary area. The

rasterized boundary covered 4,592.5434 km², leaving 12.7278 km² outside the complete valid-data mask. Flow accumulation reconciled to 5,100,539 valid DEM cells at the drainage outlets. Table 1 summarizes the input rasters, and Table 2 shows their observed ranges and modelling responses.

Figures 4–10 present the spatial distributions of the seven conditioning factors: slope (Figure 4), rainfall (Figure 5), DEM-derived topographic wetness index (TWI; Figure 6), drainage density (Figure 7), normalized difference vegetation index (NDVI; Figure 8), elevation (Figure 9), and aspect (Figure 10). The maps show greater terrain variation in southern and central Anambra, while broad lower-relief landscapes occur in northern and western areas. Rainfall and vegetation also vary spatially. Aspect is represented by compass sectors and a flat class.

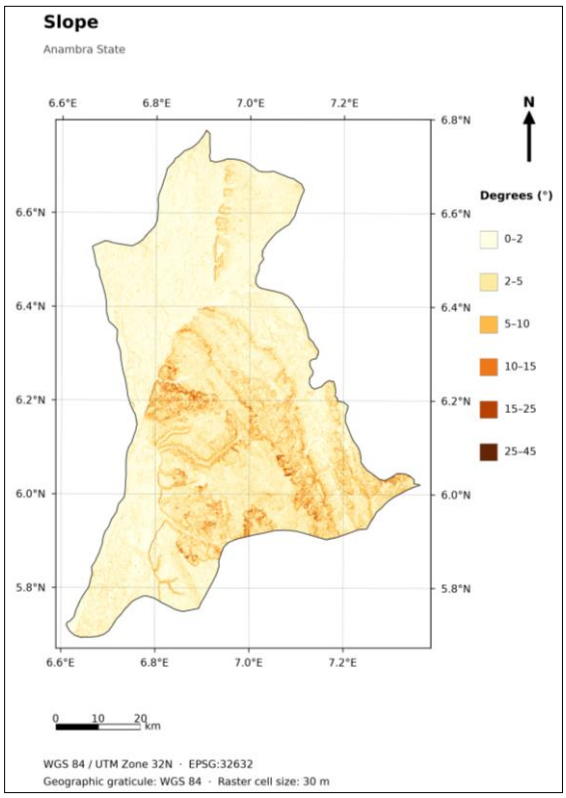


Fig 1: Spatial distribution of slope across Anambra State.

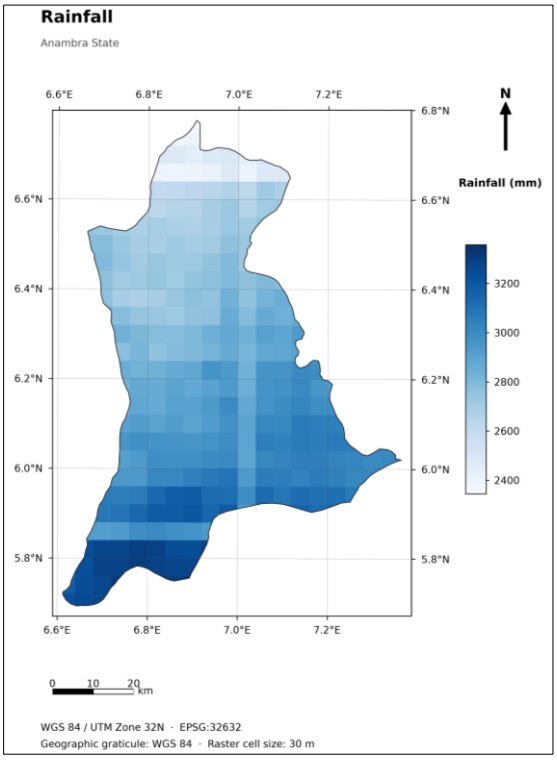


Fig 2: Spatial distribution of CHIRPS rainfall values for 2025 across Anambra State.

3.2. MEREC Weights

Table 3 and Figure 1 show the MEREC removal effects and normalized criterion weights. Rainfall had the highest weight (0.190530), followed by drainage density (0.183486), NDVI (0.176849), TWI (0.164416), local relief (0.150237), and slope (0.134483). Aspect received a zero weight because its standardized values were constant. The six varying criteria had positive removal effects, and all criterion weights sum to 1.000.

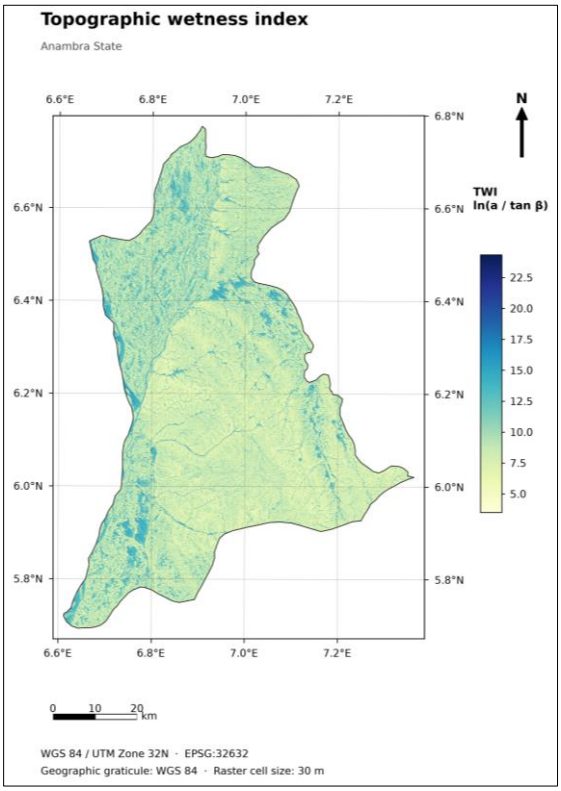


Fig 3: DEM-derived topographic wetness index across Anambra State.

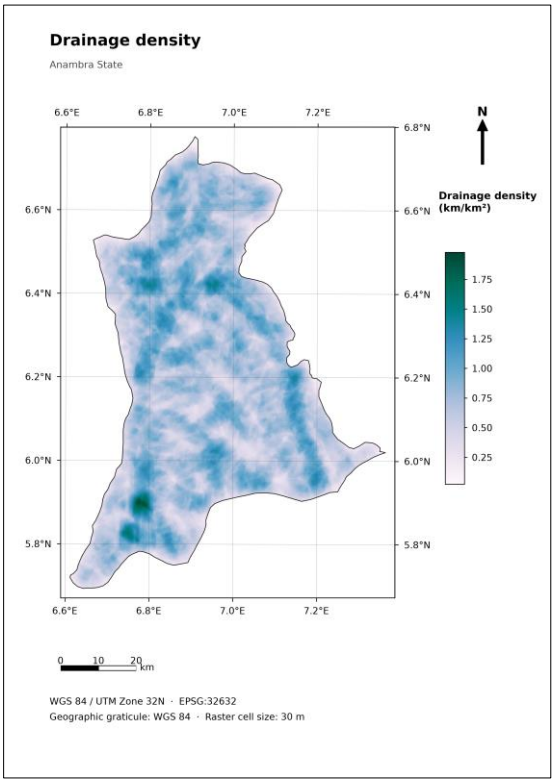


Fig 4: Spatial distribution of drainage density across Anambra State.

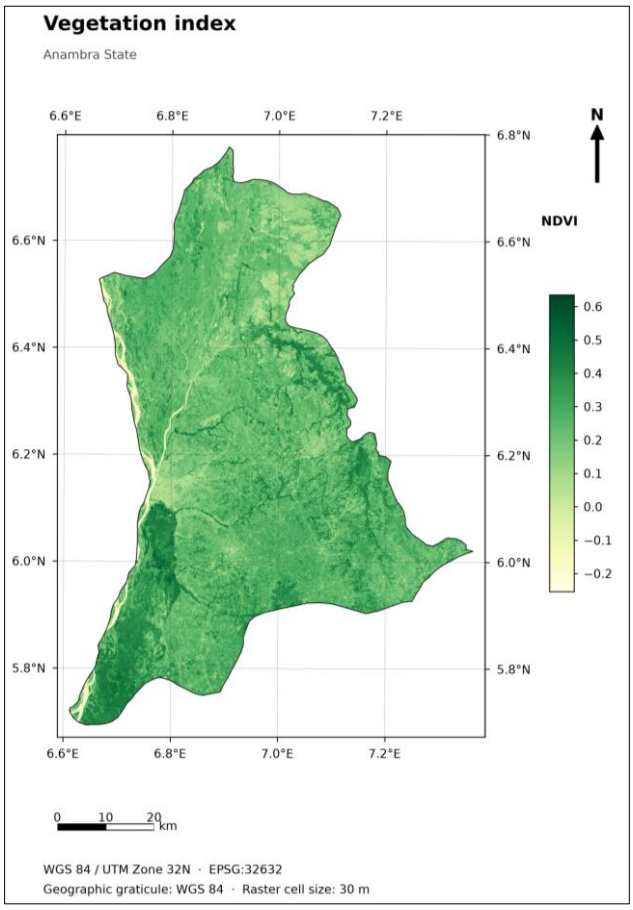


Fig 5: Spatial distribution of NDVI across Anambra State.

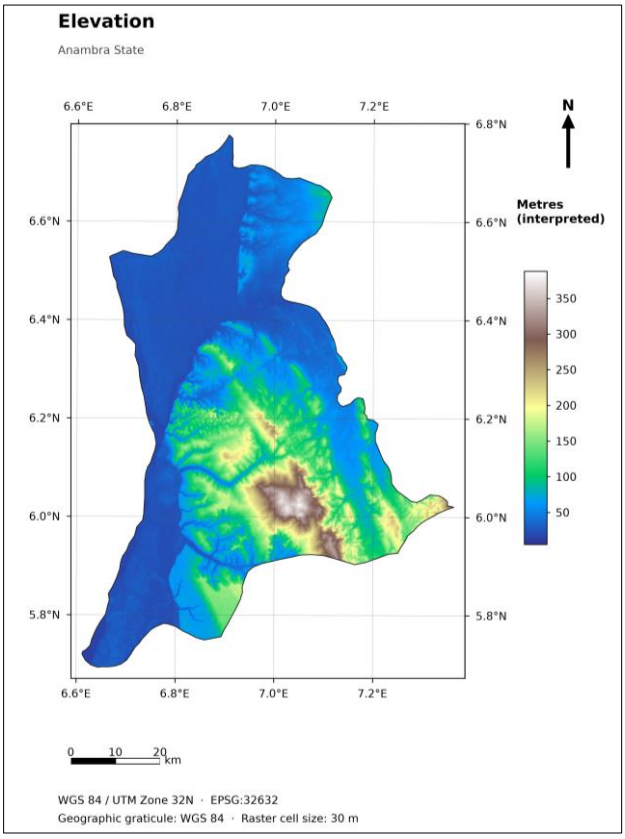


Fig 6: Elevation distribution across Anambra State.

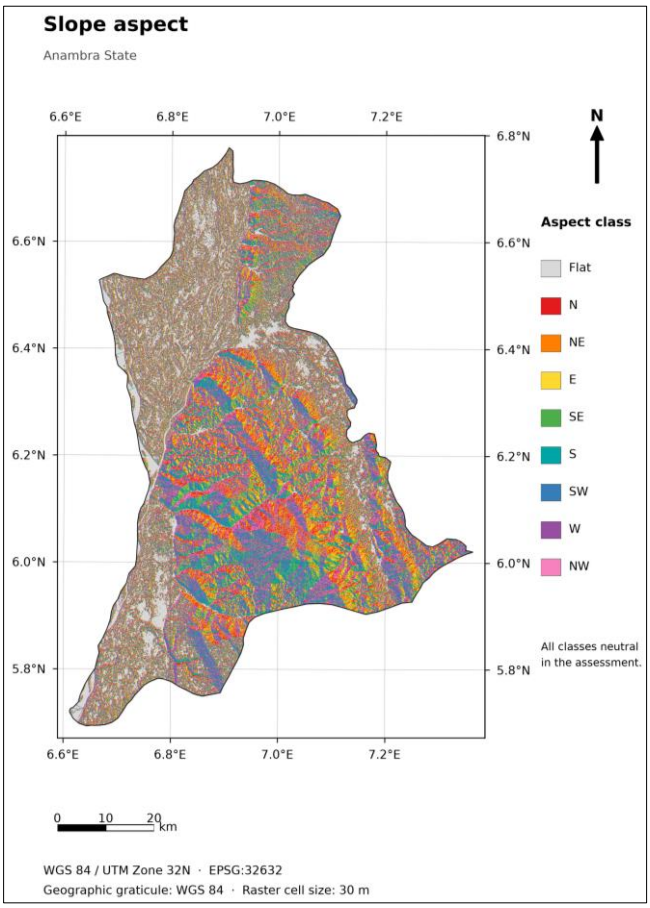


Fig 7: Aspect classes across Anambra State.

Table 3: All-cell MEREC removal effects and normalized weights.

Criterion	Removal effect E	Weight
Slope	608,101.410	0.134483
Rainfall	861,533.688	0.190530
TWI	743,454.577	0.164416
Drainage Density	829,682.129	0.183486
NDVI	799,672.987	0.176849
Elevation-derived local relief	679,337.775	0.150237
Aspect	0.000	0.000000

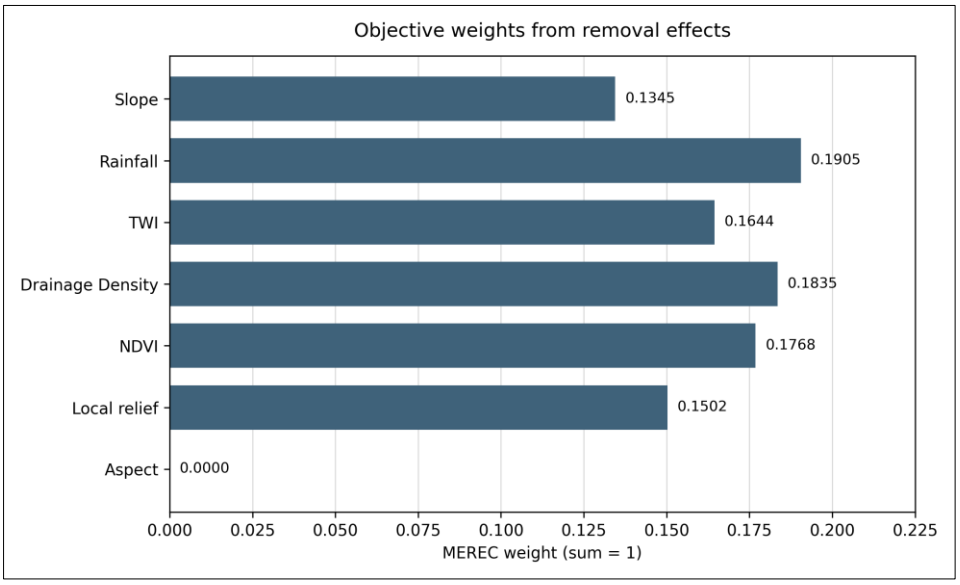


Fig 8: MEREC weights for the seven model criteria; elevation is represented by local relief.

3.3. Continuous Index and Susceptibility Zones

The continuous LSI ranged from 0.059135 to 0.776930. Its quintile boundaries were 0.301204, 0.348044, 0.389910, and 0.439736. Table 4 reports the index intervals and areas for the five classes. High and Very High zones together covered 1,831.9266 km², representing 40% of the modelled area under the quantile classification. Figure 2 shows the continuous index, while Figure 3 shows the resulting five susceptibility zones.

The mapped index shows broad lower-score areas in the north and west and larger concentrations of higher scores in southern and central Anambra. Mean slope increased from 1.617° in the Very Low zone to 4.295° in the Very High zone. Mean NDVI decreased from 0.2693 to 0.2206, while mean TWI increased from 8.029 to 9.156. Mean drainage-density values increased from 0.6052 to 0.8515, and mean rainfall-pattern values rose from 2,701.56 to 3,025.24 in their respective source units.

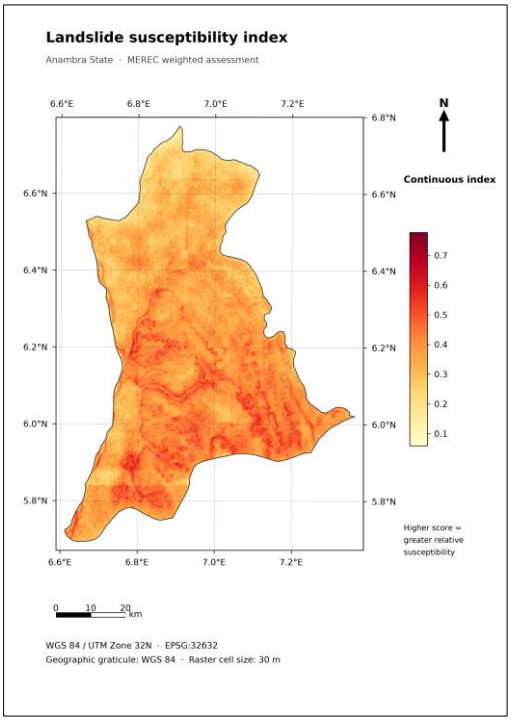


Fig 9: Continuous MEREC landslide susceptibility index across the common analysis mask.

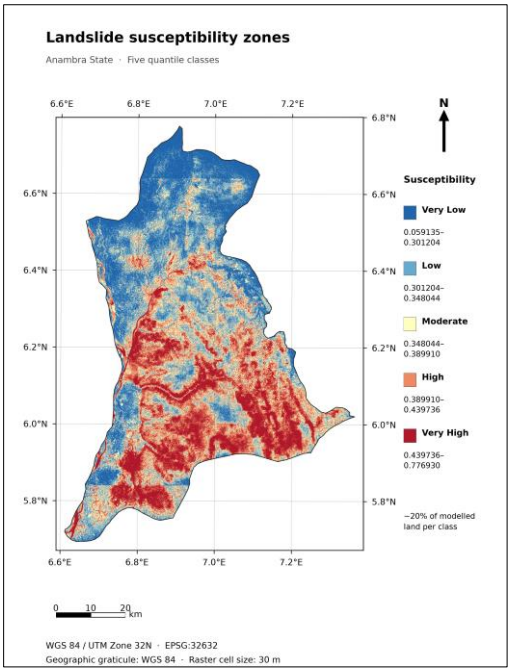


Fig 10: Five MEREC-derived landslide susceptibility zones using quintile classification.

3.4. Local Government Area Distribution

Table 5 shows susceptibility-zone areas for all 21 LGAs. Orumba North had the largest Very High area (133.4772 km²), followed by Orumba South (99.0630 km²) and Ihiala (85.2786 km²). The largest combined High and Very High areas occurred in Orumba North (240.9021 km²), Anambra East (174.8970 km²), and Orumba South (163.5156 km²). Nnewi South had the highest within-LGA Very High proportion at 48.92%, followed by Nnewi North at 41.75% and Ihiala at 38.68%. These values distinguish absolute zone area from the proportion of each LGA.

3.5. Sensitivity Analysis

Table 6 summarizes the four sensitivity scenarios. Excluding rainfall produced a Spearman correlation of 0.8456 with the baseline and 50.96% class agreement. Excluding local relief produced 53.87% class agreement. Removing rainfall and local relief together reduced correlation to 0.5799 and retained 49.31% of baseline Very High cells in that class. Raising the positive floor to 0.01 produced 95.66% class agreement and a correlation of 0.9991. The scenario analysis identifies rainfall and local relief as the criteria with the strongest effects on the mapped class configuration.

Raster-zone cells, polygonized zones, and LGA-assigned cells each accounted for 4,579.8156 km². All modelled cells were assigned to an LGA. Polygonization retained 647,293 four-connected components. The maximum difference between the saved float32 index and the repeated float64 weighted sum was 2.98×10^{-8}. Raster alignment and common-mask checks passed for all model factors.

4. Discussion

4.1. Spatial Pattern and Regional Process Context

The concentration of higher susceptibility scores in southern and central Anambra is consistent with the region's dissected terrain and the documented influence of rainfall infiltration on slope stability. Nanka-area studies describe shallow failures associated with steep slopes, poorly consolidated sandy materials, less permeable layers, and groundwater conditions (Igwe & Una, 2019; Ibeh, 2020) [8, 9]. State-wide geospatial results from southern Anambra likewise identify terrain, rainfall, vegetation, drainage, and geology as relevant conditioning variables (Nwazelibe & Egbueri, 2024) [14]. The present spatial pattern therefore aligns with the regional process setting represented by the model factors.

Rainfall had the largest MEREC weight, while drainage density and NDVI ranked second and third. This ordering reflects each criterion's removal effect across the spatial decision matrix. It describes the contribution of the prepared raster distributions to the index and should be interpreted alongside the model's factor response and spatial scale. Comparative studies of objective weighting similarly show that weights influence multicriteria spatial prioritization (Keshavarz-Ghorabaee *et al*., 2021; Mahmoodi *et al*., 2023) [10, 13].

Slope, TWI, drainage density, rainfall, and NDVI represent complementary terrain, hydrological, climatic, and vegetation conditions. The increasing means of slope, TWI, drainage density, and rainfall from Very Low to Very High zones, together with declining NDVI, show that the classified index captures the intended combination of susceptibility-oriented factor responses. TWI represents terrain-based moisture convergence rather than measured soil moisture, and its spatial pattern reflects the DEM routing and resolution used in its derivation (Riihimäki *et al*., 2021; Winzeler *et al*., 2022) [16, 22].

4.2. Factor Maps and Spatial Support

The factor distributions in Figures 4–10 provide the spatial context for the index. Slope and local relief are more pronounced in parts of the southern and central study area, while the rainfall, drainage-density, and NDVI layers contribute additional spatial contrasts. The common 30 m grid provides a consistent overlay framework. The CHIRPS rainfall raster retains its original spatial information after alignment, and the harmonized map should be interpreted at the scale of its source data.

The DEM-derived TWI provides a consistent terrain-based wetness indicator, while local relief describes elevation variation within a 990 m neighbourhood. These measures capture different aspects of terrain form and water convergence. Their sensitivity scenarios demonstrate that their inclusion affects the spatial distribution and class membership of the final index.

4.3. Model Interpretation and Planning Relevance

The index ranks the modelled landscape into five quintile-based susceptibility classes, supporting comparison across the state and identification of areas for field reconnaissance and detailed slope assessment.

The LGA summaries provide a practical basis for organizing field reconnaissance and prioritizing detailed geomorphological and geotechnical investigation. Orumba North, Orumba South, Ihiala, Nnewi South, and Anambra East contain substantial Very High or combined High and Very High areas. These mapped priorities can be integrated with geological information, infrastructure, settlement patterns, and landslide inventories to guide site-specific planning and slope management.

The study contributes a reproducible application of MEREC to state-wide landslide susceptibility mapping in Anambra State. The workflow links standardized environmental factors, all-cell objective weighting, continuous index generation, five-zone classification, and LGA-level area summaries. The resulting maps provide a consistent spatial baseline for future landslide inventory development and regional environmental planning.

5. Conclusion

This study produced a MEREC-based landslide susceptibility index and five mapped susceptibility zones for 4,579.8156 km² of Anambra State. The all-cell analysis assigned the largest criterion weight to rainfall (0.190530), followed by drainage density (0.183486) and NDVI (0.176849). High and Very High zones together covered 1,831.9266 km². Orumba North had the greatest Very High area (133.4772 km²) and combined High and Very High area (240.9021 km²), while Nnewi South had the largest within-LGA Very High proportion (48.92%). These outputs identify clear geographic priorities for field reconnaissance and detailed slope assessment.

The study demonstrates how MEREC integrates terrain, rainfall, drainage, and vegetation layers into a transparent, reproducible susceptibility index. Sensitivity analysis confirms the influence of rainfall and local relief on the mapped zones, while the LGA summaries translate the state-

wide pattern into actionable administrative priorities. Together, the susceptibility map, factor distributions, and LGA statistics provide a strong spatial foundation for regional land-use planning, slope management, and landslide risk reduction in Anambra State.

References

1. Abdelkader MM, Csámer Á. Comparative assessment of machine learning models for landslide susceptibility mapping: a focus on validation and accuracy. Natural Hazards. 2025;121(9):10299-10321. doi:10.1007/s11069-025-07197-0
2. Akosah S, Gratchev I, Kim DH, Ohn SY. Application of artificial intelligence and remote sensing for landslide detection and prediction: Systematic review. Remote Sensing. 2024;16(16):2947. doi:10.3390/rs16162947
3. Alvioli M, Marchesini I, Reichenbach P, Rossi M, Ardizzone F, Fiorucci F, *et al*. Automatic delineation of geomorphological slope units with r.slopeunits v1.0 and their optimization for landslide susceptibility modeling. Geoscientific Model Development. 2016;9(11):3975-3991. doi:10.5194/gmd-9-3975-2016
4. Claverie M, Ju J, Masek JG, Dungan JL, Vermote EF, Roger JC, *et al*. The Harmonized Landsat and Sentinel-2 surface reflectance data set. Remote Sensing of Environment. 2018;219:145-161. doi:10.1016/j.rse.2018.09.002
5. Condon LE, Maxwell RM. Modified priority flood and global slope enforcement algorithm for topographic processing in physically based hydrologic modeling applications. Computers & Geosciences. 2019;126:73-83. doi:10.1016/j.cageo.2019.01.020
6. Funk C, Peterson P, Landsfeld M, Pedreros D, Verdin J, Shukla S, *et al*. The climate hazards infrared precipitation with stations-a new environmental record for monitoring extremes. Scientific Data. 2015;2(1):150066. doi:10.1038/sdata.2015.66
7. Gorelick N, Hancher M, Dixon M, Ilyushchenko S, Thau D, Moore R. Google Earth Engine: Planetary-scale geospatial analysis for everyone. Remote Sensing of Environment. 2017;202:18-27. doi:10.1016/j.rse.2017.06.031
8. Ibeh CU. Effect of changing groundwater level on shallow landslide at the basin scale: A case study in the Odo basin of south eastern Nigeria. Journal of African Earth Sciences. 2020;165:103773. doi:10.1016/j.jafrearsci.2020.103773
9. Igwe O, Una CO. Landslide impacts and management in Nanka area, Southeast Nigeria. Geoenvironmental Disasters. 2019;6(1):5. doi:10.1186/s40677-019-0122-z
10. Keshavarz-Ghorabaee M, Amiri M, Zavadskas EK, Turskis Z, Antucheviciene J. Determination of objective weights using a new method based on the removal effects of criteria (MEREC). Symmetry. 2021;13(4):525. doi:10.3390/sym13040525
11. Kudaibergenov M, Nurakynov S, Iskakov B, Iskaliyeva G, Maksum Y, Orynbassarova E, *et al*. Application of artificial intelligence in landslide susceptibility assessment: Review of recent progress. Remote Sensing. 2025;17(1):34. doi:10.3390/rs17010034
12. Li Y, Fu B, Yin Y, Hu X, Wang W, Wang W, *et al*. Review on the artificial intelligence-based methods in landslide detection and susceptibility assessment: Current progress and future directions. Intelligent Geoengineering. 2024;1(1):1-18. doi:10.1016/j.ige.2024.10.003
13. Mahmoodi E, Azari M, Dastorani MT. Comparison of different objective weighting methods in a multi-criteria model for watershed prioritization for flood risk assessment using morphometric analysis. Journal of Flood Risk Management. 2023;16(2):e12894. doi:10.1111/jfr3.12894
14. Nwazelibe VE, Egbueri JC. Geospatial assessment of landslide-prone areas in the southern part of Anambra State, Nigeria using classical statistical models. Environmental Earth Sciences. 2024;83(7):220. doi:10.1007/s12665-024-11533-1
15. Reichenbach P, Rossi M, Malamud BD, Mihir M, Guzzetti F. A review of statistically-based landslide susceptibility models. Earth-Science Reviews. 2018;180:60-91. doi:10.1016/j.earscirev.2018.03.001
16. Riihimäki H, Kemppinen J, Kopecký M, Luoto M. Topographic wetness index as a proxy for soil moisture: The importance of flow-routing algorithm and grid resolution. Water Resources Research. 2021;57(10):e2021WR029871. doi:10.1029/2021wr029871
17. Roberts DR, Bahn V, Ciuti S, Boyce MS, Elith J, Guillera-Arroita G, *et al*. Cross-validation strategies for data with temporal, spatial, hierarchical, or phylogenetic structure. Ecography. 2017;40(8):913-929. doi:10.1111/ecog.02881
18. Roy DP, Kovalskyy V, Zhang HK, Vermote EF, Yan L, Kumar SS, *et al*. Characterization of Landsat-7 to Landsat-8 reflective wavelength and normalized difference vegetation index continuity. Remote Sensing of Environment. 2016;185:57-70. doi:10.1016/j.rse.2015.12.024
19. Shafapourtehrany M, Batur M, Özener H, Lorestani N, Kalantar B, Shabani F. Conventional and advanced geospatial techniques for landslide detection and modeling: a comprehensive overview. Geoenvironmental Disasters. 2026;13(1):3. doi:10.1186/s40677-025-00347-3
20. Valavi R, Elith J, Lahoz-Monfort JJ, Guillera-Arroita G. blockCV: An R package for generating spatially or environmentally separated folds for k-fold cross-validation of species distribution models. Methods in Ecology and Evolution. 2019;10(2):225-232. doi:10.1111/2041-210x.13107
21. Vermote E, Justice C, Claverie M, Franch B. Preliminary analysis of the performance of the Landsat 8/OLI land surface reflectance product. Remote Sensing of Environment. 2016;185:46-56. doi:10.1016/j.rse.2016.04.008
22. Winzeler HE, Owens PR, Read QD, Libohova Z, Ashworth A, Sauer T. Topographic wetness index as a proxy for soil moisture in a hillslope catena: Flow algorithms and map generalization. Land. 2022;11(11):2018. doi:10.3390/land11112018
23. Wulder MA, Loveland TR, Roy DP, Crawford CJ, Masek JG, Woodcock CE, *et al*. Current status of

Landsat program, science, and applications. Remote Sensing of Environment. 2019;225:127-147. doi:10.1016/j.rse.2019.02.015
24. Yamazaki D, Ikeshima D, Tawatari R, Yamaguchi T, O'Loughlin F, Neal JC, *et al*. A high-accuracy map of global terrain elevations. Geophysical Research Letters. 2017;44(11):5844-5853. doi:10.1002/2017gl072874
25. Zhao X, Zhao Z, Huang F, Huang J, Yang Z, Chen Q, *et al*. Application of environmental variables in statistically-based landslide susceptibility mapping: A review. Frontiers in Earth Science. 2023;11:1147427. doi:10.3389/feart.2023.1147427

How to Cite This Article
Igbokwe, O.I, Ono, M.N, Emengini, E.J, *et al*. GIS based landslide susceptibility modelling in Anambra state Nigeria using MEREC objective weighting. Int J Multidiscip Res Growth Eval. 2026;7(6):237-248.

Creative Commons (CC) License
This is an open access journal, and articles are distributed under the terms of the Creative Commons Attribution NonCommercial-ShareAlike 4.0 International (CC BY-NC-SA 4.0) License, which allows others to remix, tweak, and build upon the work non-commercially, as long as appropriate credit is given and the new creations are licensed under the identical terms